

SAND2002-8409

N. R. Moody, R. A. Causey, K. L. Wilson, and D. F. Bahr, Deuterium Induced fracture of Sputter Deposited Beryllium Films, in the Proceedings of the International Conference on "Hydrogen Effects on Material Behavior and Corrosion Deformation Interactions," N. R. Moody, A. W. Thompson, R. E. Ricker, G. Was, eds., TMS, Warrendale, PA, 2003, to be published.

DEUTERIUM-INDUCED FRACTURE OF SPUTTER DEPOSITED BERYLLIUM FILMS

N. R. Moody, R. A. Causey, K. L. Wilson, and D. F. Bahr*
Sandia National Laboratories, Livermore, CA 94550
*Washington State University, Pullman, WA 99164

Abstract

In this work, we characterized the size and shape of the blisters that formed during deposition of beryllium and deuterium and of blisters induced during nanoindentation of deuterium-free films using Atomic Force Microscopy. Mechanics-based models were combined with these measurements to determine residual stresses and interfacial fracture energies in both film systems. This analysis showed that deuterium induced high compressive residual stresses in these films. These stresses drove delamination and blister formation. More importantly, the results showed that deuterium significantly lowered the interfacial fracture energy and bond strength of beryllium films on silicon substrates. These results strongly suggest that deuterium segregates to the film-substrate interface where it degrades resistance to interfacial fracture by reducing the interfacial bond strength.

Introduction

Beryllium is a prime candidate material in the design of the International Thermonuclear Experimental Reactor (ITER) where it is proposed for use in components exposed to the hot tritium plasma. [1] It has excellent thermal conductivity for steady state heat removal and a low atomic number for reducing the impact of eroded first wall atoms on plasma contamination. [2] Beryllium also has a lower affinity for tritium than other candidate materials and therefore can more effectively limit tritium inventory. [2] Nevertheless, hydrogen-isotope and radiation induced damage remains a concern. This phenomenon was clearly shown by Chernikov et al. [3], where deuterium ion implantation in beryllium films induced formation of sub-micron sized deuterium filled bubbles throughout the films.

Recently, Causey and Walsh [4] simulated the ablation and re-deposition of beryllium from a reactor wall by replacing tritium with deuterium. They showed that co-deposition of energetic deuterium ions with eroded beryllium atoms onto silicon substrates can lead to delamination and blister formation. As in previous studies, re-deposition led to formation of two blister populations ranging from sub-micron blisters to large blisters several microns in diameter. The large blisters formed only in films with low oxygen and high deuterium contents. [4]

Oxygen is a potent hydrogen-isotope trap in beryllium. In high concentrations, oxygen getters hydrogen isotopes from potential fracture paths: in low concentrations, hydrogen isotopes are free to migrate and accumulate at the film-substrate interfaces. There is also a large volume mismatch between deuterium and beryllium during co-deposition that can create high compressive residual stresses in the film. The segregation of hydrogen at film-substrate interfaces can degrade interfacial bond strength while high residual stresses can drive delamination and blister formation. This study was conducted to define the role of deuterium in delamination and blister formation in these films.

Materials

The films used in this study were sputter deposited from a 5 cm diameter S-65 beryllium target disk by 100 eV deuterons. The sputtered beryllium was collected on heated 0.5 cm diameter polished silicon catcher plates located 5 cm in front of the beryllium disk and 5 cm from the centerline of the disk at temperatures of 423 K and 473 K. For the experiment performed with the silicon catcher plates at 473 K, the 100 eV deuteron flux was maintained at $3.3 \times 10^{23} \text{ D/m}^2\text{s}^{-1}$ uniformly over the 5 cm diameter target disk. For the experiment performed with the catcher plate at 423 K, the particle flux on the target disk was maintained at $9.9 \times 10^{23} \text{ D/m}^2\text{s}^{-1}$. [4]

The samples were then transferred to a standard scattering analysis chamber of the EN Series Tandem Van de Graff accelerator. To profile oxygen in the film systems, elastic recoil detection was then used to depth profile the concentrations of beryllium, deuterium, hydrogen and carbon. The results are given in Table I. It should be noted that Atomic Force Microscopy and nanoindentation provided film thickness values about 25 percent less than those originally estimated from elastic recoil data.

The volume mismatch on adding deuterium to beryllium can create compressive biaxial stresses in these films. To first order, the in-plane stresses can be estimated from, [5,6]

$$\sigma = \frac{E \Delta V}{3(1 - \nu)} \quad (1)$$

where the volumetric strain, Δ , is a function of the partial molar volumes of deuterium, V_D , and beryllium, V_{Be} , and the ratio between deuterium and beryllium concentrations, D/Be , as follows,

$$\Delta = \frac{V_H}{V_{Be}} \frac{D}{Be} \quad (2)$$

In these equations, σ_r is the residual stress and E and ν are the elastic modulus and Poisson's ratio for beryllium respectively. With E equal to 305 GPa, ν equal to 0.075, V_{Be} equal to 4.87 cm³/mole [2] and V_D set at 1.8 cm³/mole [8,9], the calculated stresses range from 2.8 GPa to 4.1 GPa for these films. Although these are upper bound values calculated assuming all deuterium in the films stress the lattice with no limitations imposed by film strength, they clearly show that deuterium can induce very high residual compressive stresses in these films.

Experimental Procedure

Scanning Auger Microscopy (SAM) was used to characterize the near surface and through thickness composition profiles of the films. It was also used to characterize the composition of the blistered film interfaces. Following compositional analysis, mechanical properties were determined for each film system using the continuous stiffness measurement option with a Berkovich diamond indenter on a Nano Indenter IITM. All measurements were conducted at an excitation frequency of 45 Hz and displacement of 3 nm. [10,11]

As a baseline reference, nanoindentation was used to induce blisters in the 90 nm thick beryllium film four years after deposition. This film exhibited no evidence of blister formation following film deposition. SAM and Secondary Ion Mass Spectroscopy (SIMS) further showed that there was no measurable deuterium remaining in the film or along the film-substrate interfaces four years after deposition. For the nanoindentation tests, a conical diamond indenter with a nominal one μ m tip radius and a 90° included angle was driven into the 90 nm thick beryllium film to maximum loads of ranging from 1.0 to 7.0 mN at a loading rate of 0.05 s⁻¹ using a Hysitron TriboscopeTM. During each test, the normal loads and displacements were continuously recorded. Following nanoindentation, Atomic Force Microscopy was used to determine blister morphologies in the Be films. It was also used to characterize blister morphologies in the Be-D films. The blister heights and diameters were then used to determine interfacial fracture energies from mechanics based models for circular blister formation. [12-14]

Table I. Film deposition temperatures, film thickness, and oxygen to beryllium and deuterium to beryllium concentrations. [4]

| Film Deposition Temperature | h (nm) | O/Be | D/Be |
|-----------------------------|--------|-------|------|
| 473 K | 90 | 0.125 | 0.07 |
| 423 K | 280 | 0.030 | 0.10 |

Results

Film Characterization

Composition of the sputter deposited films was determined using Scanning Auger Microscopy. The composition depth profile for the 280 nm thick Be-D film is given in Figure 1a. This figure clearly shows a 10 nm thick surface oxide on the sputter deposited beryllium film with a three atomic percent oxygen concentration through the film thickness on the silicon substrate. The beryllium film was not deposited directly on the silicon but on a silica surface layer.

Mechanical Properties

Figure 2 gives the biaxial modulus (M) and the hardness values for the 280 nm thick film as a function of indenter depth determined from nanoindentation with the biaxial modulus equal to $E/(1-\nu^2)$. It should be noted that the modulus of beryllium in the c-axis or basal normal direction is much higher than in other orientations. [15,16] The increase in near surface modulus and hardness values to a depth of 10 nm, clearly show the presence of a native surface oxide. The values then decrease with depth due to the increasing contribution of substrate properties to measured values. [17,18] When corrected for substrate effects, the modulus values for the surface oxide layer and the beryllium film are in good agreement with literature values for oxide and bulk counterparts. [7,19]

The moduli are similar in all films. However, the hardness varies inversely with film thickness from an average maximum value of 34 GPa in the 90 nm thick beryllium film to 21 GPa in the 280 nm thick film. Following the $H/3$ relationship between hardness and yield strength observed by Tabor [20], the yield strengths of these thin films are much higher than the 2.0 GPa yield strength projected for 200 nm grain size beryllium. [21] However, values near 2.0 GPa are for bulk samples where basal slip controls deformation. [22] Sputter deposited films have a basal normal texture which precludes deformation on basal and prismatic planes during indentation. This texture forces deformation to occur along pyramidal planes which are the only planes that can accommodate c-axis compression. [22,23] This mode of deformation is shown schematically

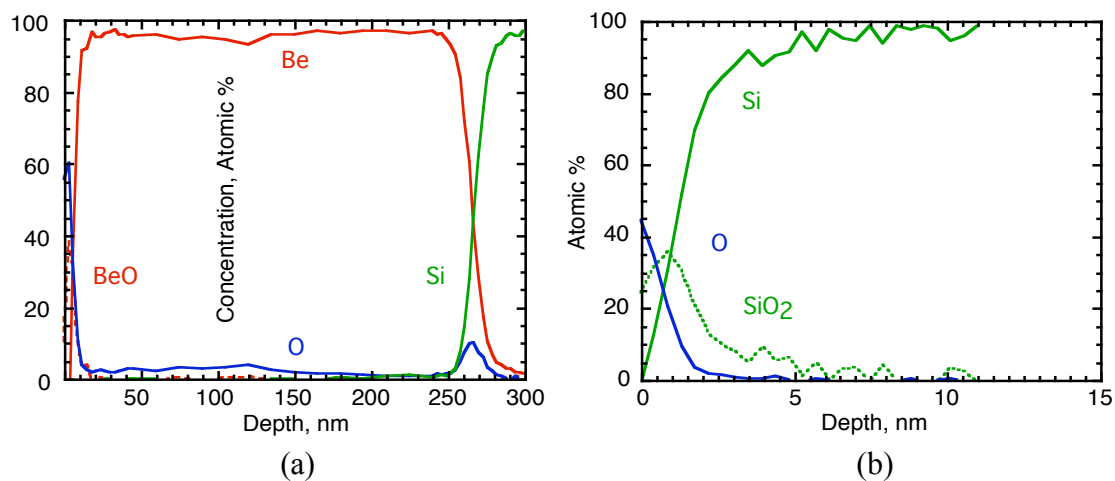


Figure 1: Composition versus depth profiles of (a) Be on silicon show that beryllium was deposited on the silicon dioxide surface of the substrate. The composition of the (b) spalled surface showed no evidence of beryllium.

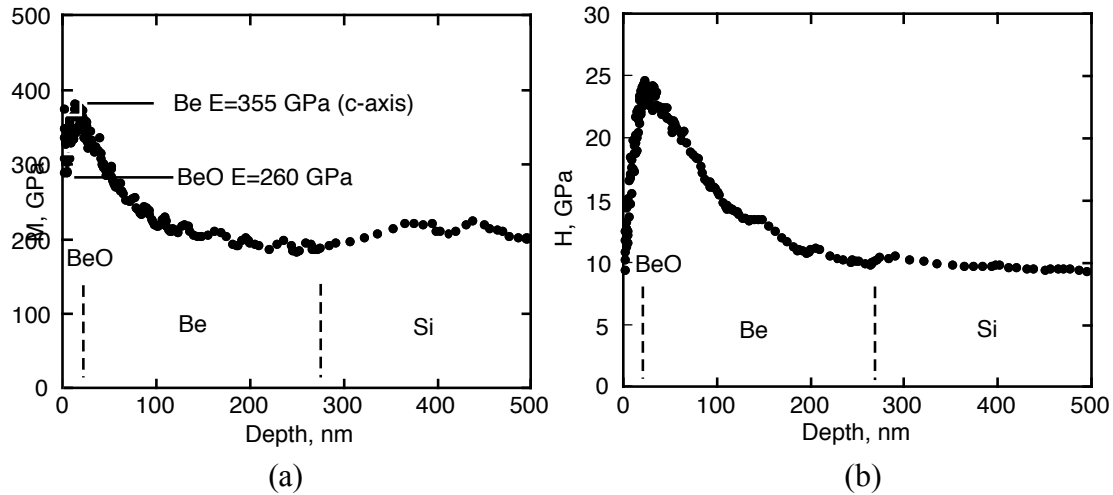


Figure 2: The (a) elastic modulus and (b) hardness values clearly show the presence of a surface oxide on the beryllium film. The modulus values correspond to c-axis properties. The hardness shows that deformation is very difficult.

in Figure 3. [24,25] The critical resolved shear stress on these planes is at least as high as for slip on prismatic planes which is six times higher than for slip on basal planes. [22,23] This analysis gives an upper bound yield strength of 12 GPa in the beryllium films. The values from nanoindentation are within this upper bound and indicate that slip on pyramidal planes controls deformation in these films.

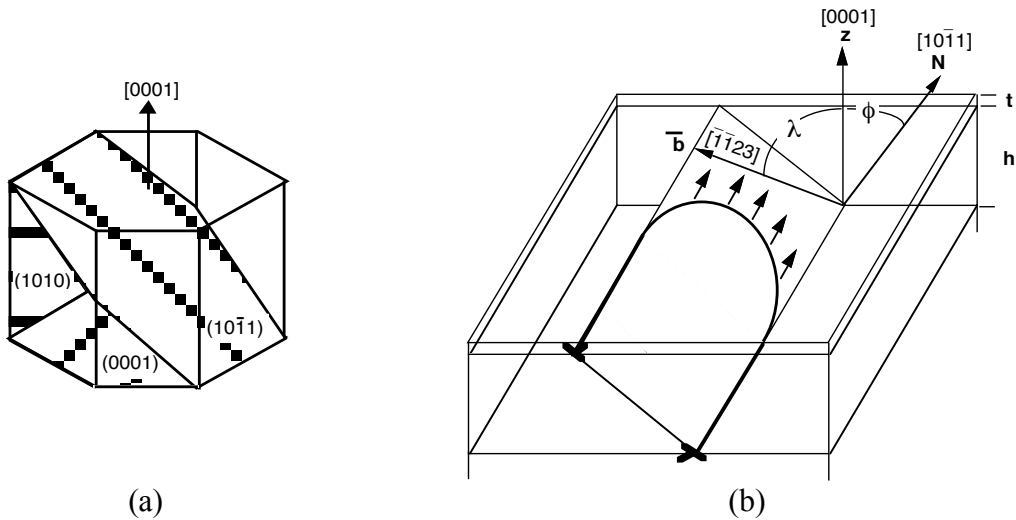


Figure 3: The beryllium films are oriented for slip on pyramidal planes as shown (a) crystallographically and by (b) a schematic of slip following the work of Freund [24] and Nix [25]

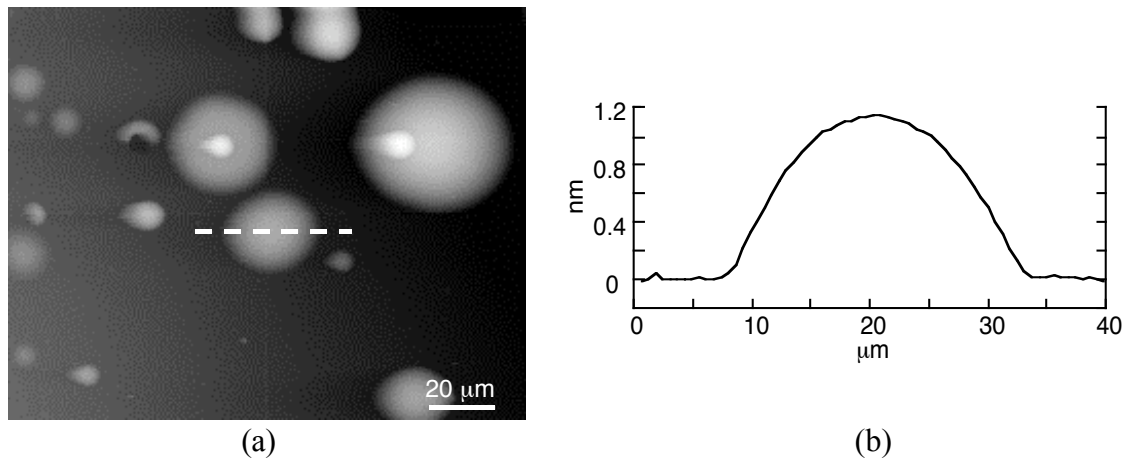


Figure 4: (a) Two populations of blisters formed in co-deposited beryllium-deuterium films with a D/Be concentration of 0.10. (b) An AFM trace across a large population blister showing the relationship between blister height and blister diameter.

Fracture

Atomic Force Microscopy revealed that co-deposition of beryllium and deuterium produced two broad populations of blisters in the 280 nm thick film; small blisters which remained intact and large blisters ranging from less than 10 μm to more than 60 μm in diameter. (Figure 4) The large blisters spalled readily from the samples during handling. It was apparent from the observations that the small blisters formed at various depths within the deposited films with some small blisters even forming on large blisters. Scanning Auger Microscopy of the substrate surface under several large spalled blisters showed no trace of beryllium indicating that failure occurred by delamination of the beryllium film from the substrate. (Figure 2b) Gas analysis during sputter depth profiling of several large blisters detected no residual deuterium. However, the delay between deposition and analysis may have allowed deuterium to off-gas.

Nanoindentation was then used to induce blisters in a 90 nm thick beryllium film. Tests at maximum loads equal to and greater than 3 mN induced blisters that increased in size with increasing load. The load versus displacement trace and corresponding blister for the test run to a maximum load of 6 mN are shown in Figure 5. In this plot, displacement values are a combination of elastic and plastic contributions from the indentation process. The discontinuity in the loading portion of the curve corresponds to the beryllium film-silicon substrate interface while the discontinuity during unloading appears to correspond to film delamination. The observations indicate that delamination is driven by stresses induced in the film from displacement of beryllium during indentation with larger displacements creating larger blisters.

Fracture Energy Analysis

The circular blisters provide data from which interfacial fracture energies can be estimated using solutions for film systems where residual stresses drive fracture behavior. [12-14] In this study, residual stresses are created during co-deposition of beryllium and deuterium and by indentation. These solutions were derived based on the assumption that the film and substrate are elastic isotropic solids, the film is subject to a uniform, equibiaxial compressive in-plane stress and the film thickness is much less than the buckle diameter.

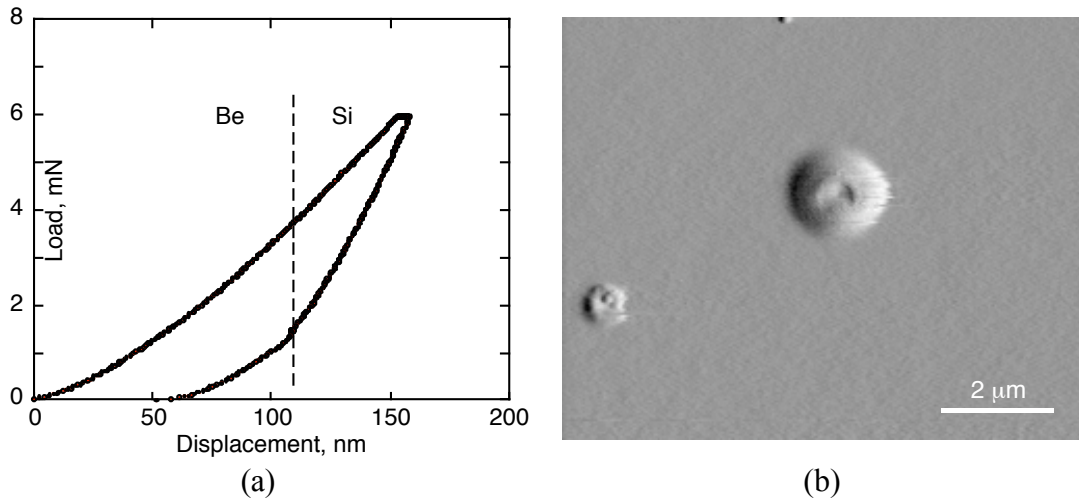


Figure 5: The (a) load versus displacement trace and corresponding (b) circular blister for indentation to a maximum load of 6 mN in the 90 nm thick beryllium film.

Blisters form when the residual compressive stress from film deposition or indentation equals or exceeds the stress for delamination. For circular blisters, the stress for delamination, σ_c , is given by [12-14],

$$\sigma_c = \frac{kE}{12(1-\nu^2)} \frac{h^2}{a^2} \quad (3)$$

where E is the elastic modulus of the film, ν is Poisson's ratio of the film, h is the film thickness, and a is the blister radius. The constant k equals 14.68 when the center is unconstrained and 42.67 when the center point is pinned. [12-14] AFM showed that the blisters formed in this study are unconstrained.

The residual stress in the Be-D film, σ_r , can then be determined from the blister height, Δ , and the stress for delamination as follows [12],

$$\sigma_r = \sigma_b \left[C \frac{\Delta^2}{h^2} + 1 \right] \quad (4)$$

where $C = 0.2473(1+\nu) + 0.2231(1-\nu^2)$. Previous studies [26,27] show that values from this approach agree with corresponding wafer curvature and x-ray diffraction measurements.

Combining blister height and radius measurements for the large blister population in the Be-D films with elastic modulus of 305 GPa and Poisson's ratio of 0.075 for beryllium, [7] provided a compressive residual stress of 1.6 ± 0.7 GPa in the 280 nm thick film. This value is well under the upper bound stress calculated from deuterium volume mismatch and the measured yield strength of the film and the substrate. It is also on the same order as stresses observed in many oxide, nitride and carbide film systems. [26,28-30]

The residual stress and stress for delamination were then used to determine the strain energy release rate for interfacial fracture as follows, [12]

$$\Gamma(\sigma) = \frac{(1 - \nu^2) h \sigma_r^2}{E [1 + 0.9021(1 - \nu^2)]} \left[\frac{r}{c} \right] \quad (5)$$

Substituting appropriate values into equation (5) gives an average interfacial fracture energy of $1.4 \pm 0.9 \text{ J/m}^2$. These values are given in Table II along with average blister heights, diameters, delamination stress and residual stress levels.

Equation (5) also provides a good approximation of fracture energies for blister formation from indentation stresses in the 90-nm-thick beryllium film. Although equations have been derived for indentation-induced stresses, [13,14] these equations do not account for significant amounts of energy dissipation from deformation and material displacement in the softer silicon substrate during indentation. As a consequence, equations based on indentation stresses overestimate fracture energies in the beryllium on silicon film system and were not included in this analysis.

Substituting appropriate values into equations (4) and (5) gives a residual stress from indentation of $4.0 \pm 0.9 \text{ GPa}$ and fracture energy of $2.5 \pm 1.2 \text{ J/m}^2$ for delamination and blister formation in the 90-nm-thick beryllium film. These values are also given in Table II. Although the average blister diameter increased with increasing indentation load and displacement, the residual stress and fracture energy values were independent of loading conditions. In addition, indentation-to-blister diameter ratios gave no indication of an interaction between the indentation and crack tip plastic zones that increase measured fracture energy values. [31] These observations indicate that the data is representative of interfacial fracture of beryllium on silicon. Comparison of these values clearly shows that deuterium has a dramatic effect on fracture energy, lowering values by a factor of two.

Interfacial fracture is often treated as a mode I failure with mode I energies, Γ_I , at crack arrest set equal to the practical work of adhesion [12,32]. This mode of failure is critical to understanding the role of deuterium in interfacial fracture of beryllium films. However, the fracture energies from equation (5) are mixed mode values consisting of shear and normal contributions. Of the criteria proposed to describe the relationship between mixed mode and mode I contributions, the following equation is often used, [12,27]

$$\Gamma_I = \Gamma(\sigma) / \cos \phi + \tan^2 \left\{ (1 - \nu^2) \sigma \right\} \left[\frac{r}{c} \right] \quad (6)$$

In this equation, σ is a material parameter equal to 0.3 and ϕ is the phase angle of loading. [12] The phase angle of loading is a measure of normal and shear force contributions to the fracture process and can be obtained using numerical solutions for circular blister formation by Hutchinson and Suo [12] as follows,

$$\phi = \tan^{-1} \left[\frac{h \Delta N}{\sqrt{12} M} \cos \psi + \frac{h \Delta N}{\sqrt{12} M} \sin \psi \right] \left[\frac{r}{c} \right] \quad (7)$$

where ΔN is the in-plane stress, M is the bending moment, and ψ is a dimensionless function describing the elastic mismatch between the film and the substrate. The value for $h \Delta N / (\sqrt{12} M)$ is determined from numerical solutions based on the loading parameter, σ_r / σ_c . [12] and ψ is set equal to 51.75° to account for elastic mismatch between the beryllium film and silica layer interface. [33] The corresponding phase angles of loading and mode I fracture energies for the

beryllium and the Be-D films are given in Table II. Comparison of these values clearly shows that deuterium has a dramatic effect on fracture energy, lowering values by a factor of three. Interestingly, this effect is similar to the effects of hydrogen on susceptibility to crack growth in iron-based alloys and in atomistic simulations of hydrogen effects on interfacial fracture of nickel. [34-38] The mode I value of $1.2 \pm 0.7 \text{ J/m}^2$ for the beryllium film on silicon corresponds well with values associated with chemical or metallic bonding. In contrast, mode I value of $0.6 \pm 0.3 \text{ J/m}^2$ for the Be-D film falls in the range of values often associated with ionic bonding. These are very hard films with essentially no deformation accompanying the interfacial fracture process.

The results suggest that deuterium promotes interfacial failure by reducing bond strength in this brittle film system. Working from the relationship for crack initiation strain energy derived by Mao [39], Volinsky et al. [31] showed that interfacial bond strength is directly related to yield strength of the film and crack initiation strain energy release rate as follows,

$$\sigma_{\text{bond}} = \frac{8}{3} \sqrt{\frac{E G_0}{\sigma_{\text{ys}} h}} \quad (6)$$

In this equation, σ_{bond} is the interfacial bond strength, G_0 is the crack initiation strain energy release rate, μ is the shear modulus, and σ_{ys} is the yield strength. Bond strengths were then calculated for the films of this study by setting the strain energy release rate equal to the measured fracture energies and substituting one-third the measured hardness values for the corresponding yield strengths. The results are given in Table II and show that the bond strength of beryllium to the silica surface layer on the silicon substrate is more than two times higher than for the Be-D film. These results strongly suggest that deuterium segregates to the film-substrate interface where it reduces the interfacial bond strength leading to delamination and blister formation.

Table II. Film thickness, blister heights, blister widths, delamination stresses, residual stresses, phase angles of loading, fracture energies and bond strengths from circular blisters in beryllium and Be-D films.

| Film | h (nm) | a (μm) | μ (μm) | σ_c (GPa) | σ_r (GPa) | $\mu(\theta)$ (J/m^2) | θ | σ_I (J/m^2) | σ_{bond} (GPa) |
|------|-----------|------------------------|----------------------------|---------------------|---------------------|-------------------------------------|----------|----------------------------------|---------------------------------|
| Be | 90 | 1.3 | 0.1 | 2.5 | -4.0 | 2.5 ± 1.2 | -62 | 1.2 ± 0.3 | 6.6 |
| Be-D | 280 | 12.3 | 1.0 | 0.3 | -1.6 | 1.4 ± 0.9 | -74 | 0.6 ± 0.3 | 3.1 |

Summary

In this study, nanoindentation and Atomic Force Microscopy were combined to define the role of deuterium on blister formation of beryllium films from silicon substrates. Nanoindentation showed that these are hard films, where deformation was forced to occur on pyramidal planes at high resolved critical shear stresses due to the basal normal texture from deposition. When co-deposited with deuterium at low oxygen contents, the large volume mismatch created high compressive residual stresses and extensive blistering along the substrate interface. Combining Atomic Force Microscopy with mechanics based models showed that the blisters formed at a mode I interfacial fracture energy of 0.6 J/m^2 . In contrast, nanoindentation was required to trigger blisters in deuterium-free films. These blisters formed at a much higher mode I interfacial fracture energy of 1.2 J/m^2 . In addition, the bond strengths were almost two times greater than for the

Be-D film. These results strongly suggest that deuterium segregates to the film-substrate interface where it reduces the interfacial bond strength. Moreover, the volume mismatch on adding deuterium to beryllium provides the driving force for spontaneous delamination and blister formation in relatively thick films with high deuterium contents.

Acknowledgments

The authors thank Angela Strojny, formerly with the University of Minnesota and now with Xerox Corporation, and Christy Woodcock with Washington State University, for their technical assistance. The authors also gratefully acknowledge the support of the U. S. DOE through Contract No. DE-AC04-94AL85000.

References

1. R. A. Causey and K. L. Wilson, *J. Nuclear Materials*, 212-215 (1994) 1436.
2. K. L. Wilson, R. A. Causey, W. L. Hsu, B. E. Mills, M. F. Smith, and J. B. Whitley, *J. Vac. Sci. Technol.*, A 8 (1990) 1750.
3. V. N. Chernikov, V. Kh. Alimov, A. V. Markin, and A. P. Zakharov, *J. Nuclear Materials*, 228 (1996) 47.
4. R. A. Causey and D. S. Walsh, *J. Nuclear Materials*, 254 (1998) 84.
5. M. F. Doerner and W. D. Nix, *CRC Reviews in Solid State and Materials Sciences*, 14 (1988) 225.
6. H. A. Wriedt and R. A. Oriani, *Acta Metall.*, 18 (1970) 753.
7. *Metals Handbook*, Properties and Selection: Nonferrous Alloys and Special-Purpose Materials, vol. 2, 10th ed., ASM International, Metals Park, OH (1990)
8. J. P. Hirth, *Metall. Trans. A*, 11A (1980) 861.
9. H. Piesl, *Hydrogen in Metals*, Topics in Applied Physics, G. Alefeld and J. Volkl, eds., 28 (1978) 53.
10. B. N. Lucas, W. C. Oliver, and J. E. Swindeman, in *Fundamentals of Nanoindentation and Nanotribology*, N. R. Moody, W. W. Gerberich, N. Burnham, and S. P. Baker, eds. (*Mater. Res. Soc. Proc.*, vol. 522, Pittsburgh, PA, 1998) 3.
11. B. N. Lucas, C. T. Rosenmayer, and W. C. Oliver, in *Thin Films-Stresses and Mechanical Properties VII*, R. C. Cammarata, M. Nastasi, E. P. Busso, and W. C. Oliver, eds. (*Mater. Res. Soc. Proc.*, vol. 505, Pittsburgh, PA, 1998) 97.
12. J. W. Hutchinson and Z. Suo, in *Advances in Applied Mechanics*, J. W. Hutchinson and T. Y. Wu, eds. (Academic Press Inc., vol. 29, New York 1992) 63.
13. D. B. Marshall and A. G. Evans, *J. Appl. Phys.*, 56 (1984) 2632.
14. A. G. Evans and J. W. Hutchinson, *Int. J. Solids Struct.*, 20 (1984) 455.
15. S. F. Pugh, *Beryllium 1977*, The Royal Society, London (1977) 13/1.
16. D. J. Silversmith and B. L. Averbach, *Phys. Rev. B*, 1 (1970) 567.
17. R. B. King, *Int. J. Solids Structures*, 23 (1987) 1657.
18. A. K. Bhattacharya and W. D. Nix, *Int. J. Solids Structures*, 24 (1988) 1287.
19. P. Garrou and A. Knudsen, *Advancing Microelectronics*, 21 (1994) 6.
20. D. Tabor, *Proc. Roy. Soc. A*, 192 (1948) 247.
21. B. C. Odegard, "Examination of Several HIP, P-1 Beryllium Modifications", SAND 74-8207 (1974).
22. A. J. Stonehouse, J. A. Cerrabine, and W. W. Beaver, *Beryllium Technology*, L. McDonald Schetky and H. A. Johnson, eds., (Gordon and Breach Science Publishers, Inc., vol. 1, New York, 1966) 51.
23. F. Aldinger, *Flow and Fracture of Single Crystal*, in *Beryllium Science and Technology*, D. Webster and G. J. London, eds., (Plenum Press, vol. 1, New York 1979) 7.
24. L. B. Freund, *J. Appl. Mech.*, 54 (1987) 553.

25. W. D. Nix, *Metall. Trans. A*, 20A (1989) 2217.
26. N. R. Moody, R. Q. Hwang, S. Venkataraman, J. E. Angelo, D. P. Norwood, and W. W. Gerberich, *Acta Mater.*, 46 (1998) 585.
27. N. R. Moody, N. Yang, D. P. Adams, M. J. Cordill, D. F. Bahr, in Thin Films: Stresses and Mechanical Properties IX, C. S. Ozkan, L. B. Freund, R. C. Camarata, and H. Gao, eds. (*Mater. Res. Soc. Proc.*, vol. 695, Pittsburgh, PA, 2002) p. L7.5.1.
28. D. F. Cardinale, D. G. Howitt, K. F. McCarty, P. B. Mirkarimi, and N. R. Moody, *Diamond and Related Materials*, 5 (1996) 1295.
29. K. Messaoudi, A. Huntz, B. Lesage, C. Haut, J. L. Lebrun, and V. Ji, in Corrosion-Deformation Interactions, T. Magnin, eds., (*The Institute of Metals*, London, 1997) 319.
30. P. J. Burnett and D. S. Rickersby, *Thin Solid Films*, 157 (1988) 233.
31. A. A. Volinsky, N. I. Tymiak, M. D. Kriese, W. W. Gerberich, and J. W. Hutchinson, in Fracture and Ductile vs Brittle Behavior-Theory, Modeling, and Experiment, G. E. Beltz, R. L. Blumberg Selinger, M. P. Marder, and K-S. Kim, eds. (*Mater. Res. Soc. Proc.* vol. 539, Pittsburgh, PA 1999) 277.
32. A. G. Evans, M. Ruhle, B. J. Dalgleish, and P. G. Charalambides, in Metal-Ceramic Interfaces, M. Ruhle, A. G. Evans, M. F. Ashby, and J. P. Hirth, eds. (*Pergamon Press*, Oxford, 1990) 345.
33. Z. Suo and J. W. Hutchinson, *Mater. Sci. Engng.*, A107 (1989) 135.
34. N. R. Moody, S. L. Robinson, and M. W. Perra, in Hydrogen Effects on Material Behavior, N. R. Moody and A. W. Thompson, eds. (*TMS*, Warrendale, PA, 1990) 625.
34. N. R. Moody, S. L. Robinson, and W. M. Garrison, *Res Mechanica* 30 (1990) 143.
36. N. R. Moody, M. W. Perra, and S. L. Robinson, *Scripta Metallurgica* 22 (1988) 1261.
37. M. W. Perra, in Environmental Degradation of Engineering Materials in Hydrogen, M. R. Louthan, Jr., R. P. McNitt, and R. D. Sisson, Jr., eds. (*VPI Press*, Blacksburg, VA, 1981) 321.
38. N. R. Moody and S. M. Foiles, in Structure/Property Relationships for Metal-Metal Interfaces, A. D. Romig, D. E. Fowler, and P. S. Bristowe, eds., (*Mater. Res. Soc. Proc.* Pittsburgh, PA, vol. 229, 1991) 179.
39. S. X. Mao and A. G. Evans, *Acta Mater.*, 45 (1997) 4263.